# Live Calculation Method for the Mutual Capacitance in Capacitive Wireless Power Transfer Systems with Multiple Receivers

Aris van Ieperen, Stijn Derammelaere, Ben Minnaert

***Abstract*—Capacitive wireless power transfer shows promise for wireless energy delivery, utilizing capacitive coupling for transmission. Quantifying the coupling between individual transmitters and receivers is essential, as optimization techniques for optimal output impedance depend on accurate knowledge of the coupling coefficient. Since practical capacitive power transfer systems often experience variations in distance or alignment, impacting the coupling coefficient and consequently, the optimal output impedance, it is desired to constantly measure the coupling coefficient. However, existing methods for measuring mutual capacitance in CPT systems require specific conditions, making them unsuitable for live measurements. This paper introduces a method for live calculation of mutual capacitance in CPT systems, applicable during normal operation. We present a theoretical framework applicable to SIMO systems with an arbitrary number of receivers and validate our results experimentally for both SISO and SIMO systems using a $10\,\mathrm{W}$ prototype operating at a frequency of $1\,\mathrm{MHz}$. Our method shows strong agreement with established techniques, especially for systems with identical receivers. This approach enables live mutual capacitance calculation based on voltages and currents available during normal system operation. It is effective for SISO and SIMO configurations, confirmed by simulations and experiments.**

***Index Terms*—Coupling, CPT, SIMO, Mutual Capacitance**

## I. Introduction

Wireless power transfer (WPT) is a promising technology with the potential to significantly impact various applications, from consumer electronics to electric vehicles (EVs) and medical implants [1]–[5]. The ability to transmit power without physical connections offers numerous advantages, including enhanced convenience, increased durability and improved safety in hazardous environments.

Inductive wireless power transfer (IPT) is the leading technique in WPT [6], using magnetic fields to transfer energy. By utilizing the principle of electromagnetic induction, a time-varying current in a primary coil generates a magnetic field that induces a current in a spatially separated secondary coil. This technique, widely employed in devices like wireless charging pads for smartphones and electric vehicles [7], [8], is renowned for its high efficiency over short distances and robust power transfer capabilities [9]. Despite its efficiency, IPT systems face challenges related to alignment and distance [10], which can impact their performance in certain applications.

As an alternative, capacitive wireless power transfer (CPT) uses electric fields to transfer energy between conductive plates or electrodes. This method relies on the oscillating electric field generated between a pair of electrodes, which induces a displacement current in the receiver. CPT offers several advantages over IPT, including a lower cost, weight and heat generation, being less affected by the presence of metal objects and a higher tolerance to misalignment [11]. CPT systems have been applied in many areas, such as charging mobile devices, LED drivers, unmanned aerial vehicles, rail transportation, and vehicle charging [12]–[17].

The capacitive coupling interface in CPT systems is formed by conductive plates, and is well suited for system configurations with multiple receivers. This structure is especially advantageous in scenarios where multiple devices need to be charged simultaneously, such as in consumer electronics, where devices like smartphones, smartwatches, and earbuds can be charged together without the need for individual charging ports and cables [18], and in industrial automation, where continuous operation of multiple automated guided vehicles relies on efficient power distribution [19]. Furthermore, in dynamic electric vehicle charging, multiple receivers allow for continuous power transfer as vehicles move along a charging path. Here, CPT systems must maintain a constant output voltage despite variations in load impedance and ensure that the voltage at other receivers remains stable when a receiver is connected or disconnected [20].

In [21], a model is proposed to represent the capacitive coupling interface, which uses an equivalent mutual capacitance $C_M$ to quantify the coupling. Methods to measure this mutual capacitance are presented in [21] and [22], for single input single output (SISO) and multiple inputs multiple outputs (MIMO) systems respectively. However, these methods are applied to a specific configuration of a CPT system, and a change in distance or alignment would require a new measurement, which requires specific system states that do not occur during normal system operation, such as for instance a short circuit at the transmitter or receiver side. Therefore, these methods are not applicable for live mutual capacitance calculation.

In practical CPT systems, change in distance or alignment between the transmitter and receivers is often inevitable. With

Manuscript received xx xx, 202x; revised xx xx, 202x.

*(Corresponding author: A.I. van Ieperen.)*

Aris van Ieperen and Ben Minnaert are with the Department of Electromechanics, CosysLab, University of Antwerp, 2020 Antwerp, Belgium (e-mail: aris.vanieperen@uantwerpen.be; ben.minnaert@uantwerpen.be).

Stijn Derammelaere is with the Department of Electromechanics, CosysLab, University of Antwerp, 2020 Antwerp, Belgium and with the AnSyMo/CoSys, Flanders Make, 3920 Lommel, Belgium (e-mail: stijn.derammelaere@uantwerpen.be).

such a change in distance or alignment, the mutual capacitance varies and as a result, the efficiency and power transfer change. Optimization techniques exist for the optimal output impedance [23], [24], but these optimizations require knowledge of the mutual capacitance. Additionally, other forms of system optimization, such as matching network optimization [25], [26] and multi-objective optimization [27], also depend on mutual capacitance data. By implementing these optimizations dynamically, CPT systems can respond to changes in alignment and distance more effectively, ensuring consistent performance at a maximum efficiency. Therefore, there is a growing need for live mutual capacitance calculation in CPT systems to support these advanced optimization strategies and enhance overall system performance.

The proposed method enables live estimation of the mutual capacitance in CPT systems during normal operation, without requiring system interruptions. This capability is particularly valuable in applications where real-time adaptation and optimization are essential. For instance, in multi-device charging scenarios, where individual devices may be added or removed at any moment, the method ensures continuous monitoring, allowing dynamic optimization in response to changes. Similarly, in applications such as automated guided vehicles (AGVs) and EV charging, the method enables real-time adjustment of power transfer parameters under misalignment conditions, ensuring stable and efficient energy transfer.

While significant progress has been made in real-time parameter estimation for IPT systems, similar approaches for CPT remain largely unexplored. For instance, in SISO IPT systems, an equation establishing the relationship between inductive coupling and the output voltage was derived in [28]. State estimation techniques, in time and frequency domain, are deployed in [29], [30]. Furthermore, in [31], a method is presented to measure the cross-coupling for IPT systems with multiple receivers using only the primary current and in [32], a transmitter-side voltage-based mutual inductions estimation method has been developed for multiple input single output (MISO) systems. The comparison between the literature and the proposed coupling estimation method is summarized in Table I.

In [33], we introduced an exact method for calculating the coupling coefficient $k$, which requires the mutual capacitance $C_M$, using measured quantities that are available during normal system operation for a setup with one transmitter and two receivers. We demonstrated the method's effectiveness through simulation. In this work, we extend the theoretical derivation to N receivers and experimentally validate our results for both SISO and SIMO systems. We compare the results with measured quantities obtained by a well-established method from literature [21]. To the best of our knowledge, this is the first method proposed and experimentally validated for live calculation of the mutual capacitance for capacitive wireless power transfer systems.

Unlike traditional methods that typically require system interruptions or specific operating states, thereby limiting their applicability in optimization scenarios, this approach utilizes voltage and current measurements obtained during normal system operation. Consequently, the proposed method not only enables seamless live system optimization but also lays the groundwork for further advancements in multi-receiver CPT systems.

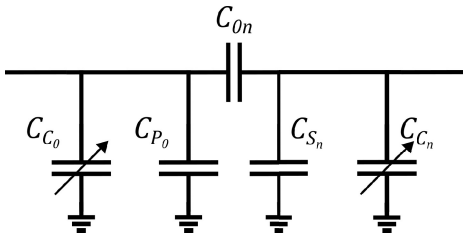


Fig. 1. Equivalent circuit representation of a SISO CPT coupling interface with controllable compensation capacitances $C_{C_0}$ and $C_{C_n}$.

## II. Methods

A CPT coupling interface can be represented by an equivalent circuit, given by a primary capacitance $C_{P_0}$ at the transmitter side and a secondary capacitance $C_{S_n}$ at the receiver side (with $n$ the number of the receiver), coupled by a mutual capacitance $C_{0n}$ [21], as shown in Fig. 1. By adding controllable compensation capacitances $C_{C_0}$ and $C_{C_n}$, a constant total capacitance on one side (e.g. $C_{C_n} + C_{S_n} + C_{0n}$ at the receiver side) can be maintained.

By adjusting the controllable capacitances, the resonance frequency $f$ can be maintained constant despite varying mutual capacitances $C_{0n}$ [34], caused by changes in distance or alignment of the coupling plates. Given the known inductances in the system, the total capacitance of the transmitter or receiver is also determined. We introduce $C_0$ and $C_n$ as this total capacitance at the transmitter and receiver sides, respectively:

$$C_0 = C_{00} + \sum_{n=1}^{N} C_{0n}, \tag{1}$$

$$C_n = C_{nn} + C_{0n}, \tag{2}$$

with N the total number of receivers, $C_{00}$ the sum of the compensation capacitance $C_{C_0}$ at the transmitter side and the primary coupling interface capacitance $C_{P_0}$, and $C_{nn}$ the sum of the compensation capacitance $C_{P_n}$ at the receiver side and the secondary coupling interface capacitance $C_{C_n}$:

$$C_{00} = C_{C_0} + C_{P_0}, \tag{3}$$

$$C_{nn} = C_{C_n} + C_{S_n}. \tag{4}$$

The method we propose determines the primary capacitance $C_{00}$ and secondary capacitances $C_{nn}$, based on current and voltage measurements during normal system operation at transmitter and receiver sides, from which the mutual capacitance $C_{0n}$ can be deducted.

However, measuring high-frequency signals presents significant challenges in practical WPT systems, particularly for voltage and current measurements. To ease the requirements for the voltage and current measurements, the derived method

TABLE I
COMPARISON BETWEEN THE PROPOSED METHOD AND THE EXISTING LITERATURE.

| Reference | IPT/CPT | Method | Operating frequency | Multiple ouputs | Transmitter/Receiver information needed | Special system states required |
|---|---|---|---|---|---|---|
| [28] | IPT | Impedance tracking | 40 kHz | No | Receiver | No |
| [29] | IPT | Time-domain state estimation | 84.5 kHz | No | Transmitter | No |
| [30] | IPT | Frequency-domain state estimation | 82 kHz | No | Transmitter | No |
| [31] | IPT | Decoupling-switch | 56.8 kHz | Yes | Transmitter | Yes |
| [32] | IPT | Voltage-based | 100 kHz | No | Transmitter | No |
| [21] | CPT | Short-circuit | 1 MHz | No | - | Yes |
| [22] | CPT | Open-circuit | 1 MHz | Yes | - | Yes |
| This work | CPT | Kirchoff | 1 MHz | Yes | Both | No |

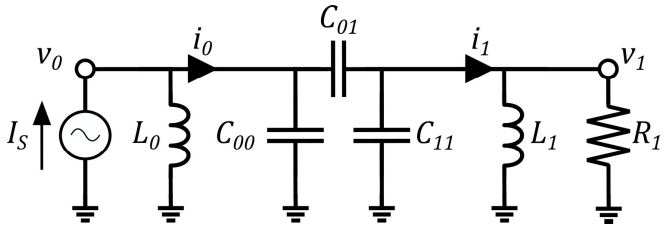


Fig. 2. Equivalent circuit representation of a SISO CPT system.

utilizes phasors, which only require amplitude and zero-crossing information. By employing phasors, the amplitude can be determined using multiple periods to calculate and average value. Techniques such as envelope detection and equivalent-time sampling have been developed for measuring high-frequency signal amplitudes [35]–[37], and zero-crossing detection can be achieved using methods like current shunts [38], [39]. Moreover, due to the Fundamental Harmonic Approximation (FHA), the voltage derivatives $dv_n/dt$, which appear in the derived equations, can be easily calculated directly from the measured voltages.

### A. SISO

We consider an ideal resonant SISO CPT system as shown in Fig. 2, with $L_0$ and $L_1$ configured to resonate with the chosen total capacitances $C_0$ and $C_1$ at the angular frequency $\omega_0$, such that $L_0 = 1/\omega_0^2 C_0$ and $L_1 = 1/\omega_0^2 C_1$, $C_{00}$ and $C_{11}$ the primary and secondary capacitances, $C_{01}$ the mutual capacitance and $R_1$ the resistive load. The transmitter is powered by a current source with peak value $I_S$ and operating frequency $f$. We measure the currents $i_0$ and $i_1$, and voltages $v_0$ and $v_1$ as defined on the figure, and represent them in phasor form using their polar representation:

$$\begin{aligned} \overline{\mathbf{I}}_0 &= I_0 e^{j\phi_{i_0}}, \qquad \overline{\mathbf{I}}_1 = I_1 e^{j\phi_{i_1}}, \\ \overline{\mathbf{V}}_0 &= V_0 e^{j\phi_{v_0}}, \qquad \overline{\mathbf{V}}_1 = V_1 e^{j\phi_{v_1}}, \end{aligned} \tag{5}$$

where $I_0$, $I_1$, $V_0$, and $V_1$ are the magnitudes, and $\phi_{i_0}$, $\phi_{i_1}$, $\phi_{v_0}$, and $\phi_{v_1}$ are the phase angles of the respective phasors.

Using Kirchhoff's current law, the current phasors of the primary $\overline{\mathbf{I}}_0$ and secondary side $\overline{\mathbf{I}}_1$ can be expressed as the current through the capacitive components as follows:

$$\overline{\mathbf{I}}_0 = \overline{\mathbf{I}}_{C_{00}} + \overline{\mathbf{I}}_{C_{01}}, \tag{6}$$

$$\overline{\mathbf{I}}_1 = \overline{\mathbf{I}}_{C_{01}} - \overline{\mathbf{I}}_{C_{11}}. \tag{7}$$

Here, $\overline{\mathbf{I}}_{C_{00}}$ represents the current through the primary capacitance $C_{00}$, $\overline{\mathbf{I}}_{C_{11}}$ represents the current through the secondary capacitance $C_{11}$, and $\overline{\mathbf{I}}_{C_{01}}$ represents the current through the mutual capacitance $C_{01}$. By combining these two equations we can derive an expression for the difference between the currents on the primary and secondary sides as a function of the currents through the primary and secondary capacitances:

$$\overline{\mathbf{I}}_0 - \overline{\mathbf{I}}_1 = \overline{\mathbf{I}}_{C_{00}} + \overline{\mathbf{I}}_{C_{11}}. \tag{8}$$

We can express these currents in terms of the capacitances and voltage phasors, using the well-known capacitor current equation, $\overline{\mathbf{I}} = C \cdot j\omega\overline{\mathbf{V}}$:

$$\overline{\mathbf{I}}_0 - \overline{\mathbf{I}}_1 = C_{00} \cdot j\omega\overline{\mathbf{V}}_0 + C_{11} \cdot j\omega\overline{\mathbf{V}}_1. \tag{9}$$

Next, we can express the primary capacitance $C_{00}$ and secondary capacitance $C_{11}$ in terms of the known values $C_0$ and $C_1$, which are the total capacitances on the transmitter and receivers sides, respectively:

$$C_{00} = C_0 - C_{01}, \tag{10}$$

$$C_{11} = C_1 - C_{01}. \tag{11}$$

Substituting the expressions for $C_{00}$ and $C_{11}$ from (10) and (11) into (9), we obtain the following equation:

$$\overline{\mathbf{I}}_0 - \overline{\mathbf{I}}_1 = C_{00} \cdot j\omega\overline{\mathbf{V}}_0 + (C_1 - C_0 + C_{00}) \cdot j\omega\overline{\mathbf{V}}_1. \tag{12}$$

This equation expresses the difference between the currents on the primary and secondary side as a function of the voltage phasors $\overline{\mathbf{V}}_0$ and $\overline{\mathbf{V}}_1$, the capacitances, and the angular frequency $\omega$. We can now isolate $C_{00}$ by rearranging the terms:

$$C_{00} = \frac{\overline{\mathbf{I}}_0 - \overline{\mathbf{I}}_1 - (C_1 - C_0) \cdot j\omega\overline{\mathbf{V}}_1}{j\omega\overline{\mathbf{V}}_0 + j\omega\overline{\mathbf{V}}_1}. \tag{13}$$

This expression allows us to calculate the primary capacitance $C_{00}$ by using measurements of the current phasors $\overline{\mathbf{I}}_0$ and $\overline{\mathbf{I}}_1$, the voltage phasors $\overline{\mathbf{V}}_0$ and $\overline{\mathbf{V}}_1$, and the known capacitances $C_0$ and $C_1$. Finally, rearranging (10) results in the following expression for the mutual capacitance $C_{01}$:

$$C_{01} = C_0 - C_{00}. \tag{14}$$

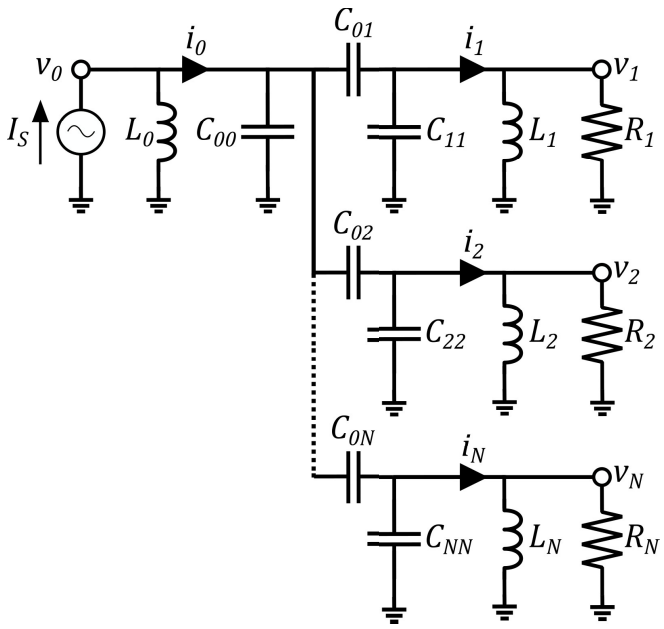


Fig. 3. Equivalent circuit representation of a SIMO CPT system with one transmitter and N receivers.

Note that the mutual capacitance $C_{01}$ can be calculated using voltages and currents that can be measured during normal system operation. Therefore, the proposed method is suitable for live calculation of the mutual capacitance in SISO CPT systems.

### B. SIMO

The method is applicable to SIMO systems with N receivers. We illustrate the methodology for a CPT system with one transmitter and N receivers, as shown in Fig. 3. Applying Kirchoff's current law results in the following equation, which relates the transmitter current $\overline{\mathbf{I}}_0$, the sum of the receiver currents $\sum_{n=1}^{N}\overline{\mathbf{I}}_n$, and the voltages across the transmitter and receivers:

$$\overline{\mathbf{I}}_0 - \sum_{n=1}^{N}\overline{\mathbf{I}}_n = C_{00}\cdot j\omega\overline{\mathbf{V}}_0 + \sum_{n=1}^{N} C_{nn}\cdot j\omega\overline{\mathbf{V}}_n, \tag{15}$$

where $C_{nn}$ respresents the individual capacitances for each receiver and can be expressed as:

$$C_{nn} = C_n - C_{0n}. \tag{16}$$

Because of the resonance condition, the ratios between the resistor currents are equal to the capacitance ratios. Using this property, we can express the mutual capacitances $C_{0n}$ as a function of the mutual capacitance between the first transmitter and receiver $C_{01}$:

$$C_{0n} = \frac{|\overline{\mathbf{V}}_n|R_1}{|\overline{\mathbf{V}}_1|R_n}C_{01}. \tag{17}$$

Substituting this expression for $C_{0n}$ into (1) gives:

$$C_0 = C_{00} + \sum_{n=1}^{N}\frac{|\overline{\mathbf{V}}_n|R_1}{|\overline{\mathbf{V}}_1|R_n}C_{01}. \tag{18}$$

This can be rearranged to isolate $C_{01}$, the mutual capacitance between the first transmitter and the first receiver:

$$C_{01} = \frac{C_0 - C_{00}}{\sum_{n=1}^{N}\frac{|\overline{\mathbf{V}}_n|R_1}{|\overline{\mathbf{V}}_1|R_n}}. \tag{19}$$

For clarity, we introduce the phasors $\overline{\mathbf{X}}_1$ and $\overline{\mathbf{X}}_2$ to simplify the notation:

$$\overline{\mathbf{X}}_1 = \sum_{n=1}^{N}\frac{|\overline{\mathbf{V}}_n|R_1}{|\overline{\mathbf{V}}_1|R_n}\frac{1}{\sum_{n=1}^{N}\frac{|\overline{\mathbf{V}}_n|R_1}{|\overline{\mathbf{V}}_1|R_n}}\cdot j\omega\overline{\mathbf{V}}_n, \tag{20}$$

$$\overline{\mathbf{X}}_2 = \sum_{n=1}^{N} C_n\cdot j\omega\overline{\mathbf{V}}_n. \tag{21}$$

Substitution of (17) and (19) in (15) gives:

$$\overline{\mathbf{I}}_0 - \sum_{n=1}^{N}\overline{\mathbf{I}}_n = C_{00}\cdot j\omega\overline{\mathbf{V}}_0 + \overline{\mathbf{X}}_2 - (C_0 - C_{00})\,\overline{\mathbf{X}}_1, \tag{22}$$

which we can rearrange as an expression of $C_{00}$:

$$C_{00} = \frac{\overline{\mathbf{I}}_0 - \sum_{n=1}^{N}\overline{\mathbf{I}}_n - \overline{\mathbf{X}}_2 + C_0\overline{\mathbf{X}}_1}{\overline{\mathbf{I}}_0 + \overline{\mathbf{X}}_1}. \tag{23}$$

We can now calculate the mutual capacitance between the transmitter and the first receiver $C_{01}$ using (19), and the mutual capacitances $C_{0j}$ between the transmitter and the other receivers using (17). Note that we can calculate these mutual capacitances using voltages and currents that can be measured during normal system operation. Therefore, the proposed method is suitable for live coupling calculation in SIMO CPT systems.

However, for systems involving not only multiple receivers but also multiple transmitter, such as a configuration with two transmitters and two receivers, the proposed method is not applicable, as it leads to an underdetermined system. Further research is needed to adapt the method for applicability in MIMO systems.

## III. Results and Discussion

### A. Circuit simulation

The analytical derivation is validated in the electric circuit simulation environment Simscape for Matlab Simulink using the equivalent circuit of a resonant CPT system with one transmitter and five receivers.

In Fig. 4, the Simscape model of the SIMO CPT system is shown. The supply at the transmitter side is represented by a current source with a frequency $f$ and peak value $I_S$. The load of each receiver is modeled as a resistor with resistances $R_n$ ($n = 1, .., 5$). The capacitive link is represented by primary $C_{00}$ and secondary capacitances $C_{nn}$, and their mutual capacitances $C_{0n}$. The inductances $L_0$ and $L_n$ are used

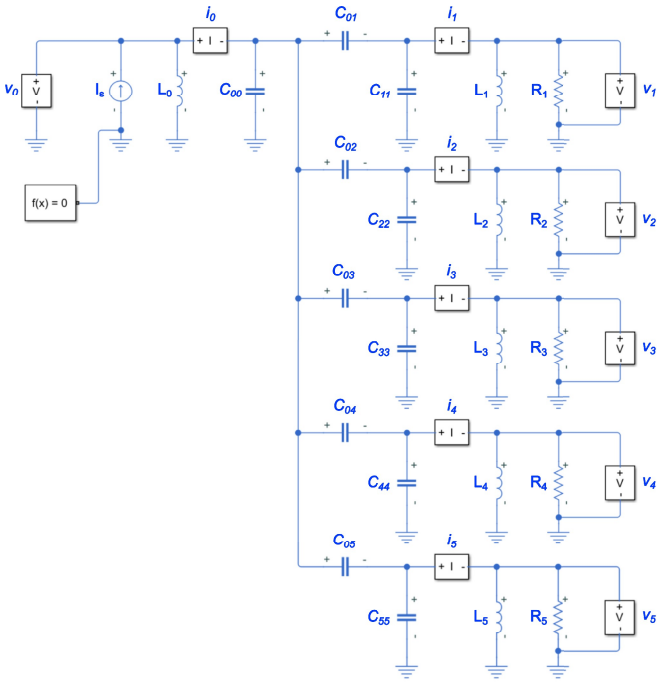


Fig. 4. Simscape model of SIMO CPT system with five receivers.

TABLE II
VALUES OF SIMULATION COMPONENTS.

| Parameter | Value | Unit |
|---|---|---|
| $C_0$ | 500 | pF |
| $C_1$ | 200 | pF |
| $C_2$ | 350 | pF |
| $C_3$ | 150 | pF |
| $C_4$ | 125 | pF |
| $C_5$ | 100 | pF |
| $f$ | 1 | MHz |
| $I_0$ | 100 | mA |
| $L_0$ | 50.66 | µH |
| $L_1$ | 126.65 | µH |
| $L_2$ | 72.37 | µH |
| $L_3$ | 168.87 | µH |
| $L_4$ | 202.64 | µH |
| $L_5$ | 253.30 | µH |
| $R_1$ | 1000 | Ω |
| $R_2$ | 500 | Ω |
| $R_3$ | 750 | Ω |
| $R_4$ | 250 | Ω |
| $R_5$ | 100 | Ω |

to create resonant circuits. The values of the parameters used in this simulation are listed in Table II.

In the simulation, the coupling coefficients are calculated for each simulation time-step, according to the following procedure: First, the primary capacitance $C_{00}$ is calculated according to (23), using the indicated current and voltage measurements. Second, the mutual capacitance between the transmitter and the first receiver is computed according to (19). Third, the mutual capacitances $C_{0n}$ are determined following (17).

The mutual capacitances $C_{0n}$ are linearly varied over a time span of 100 µs, with $C_{01}$, $C_{03}$ and $C_{05}$ decreasing

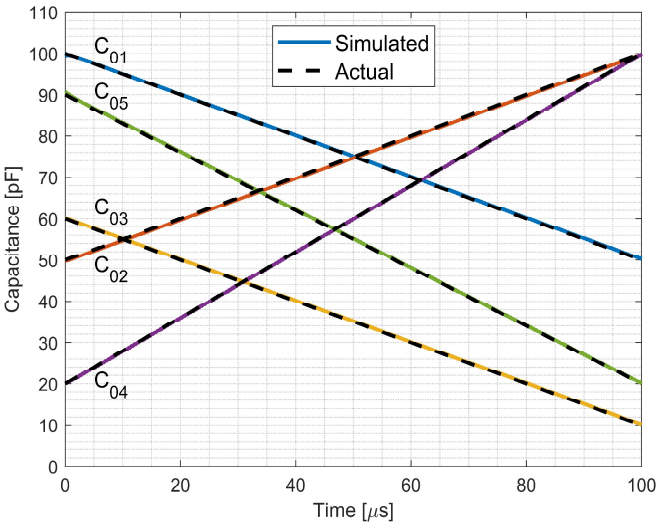


Fig. 5. Simulated (solid line) and actual (dashed line) mutual capacitances $C_{0n}$ of a SIMO CPT system with one transmitter and five receivers with varying mutual capacitances $C_{0n}$.

from 100 pF, 60 pF and 90 pF to 50 pF, 10 pF and 20 pF respectively. The other two mutual capacitances, $C_{02}$ and $C_{04}$, are increasing from 50 pF and 20 pF to 100 pF.

Using the proposed method, the mutual capacitances $C_{0n}$ are calculated using the simulation results, and compared with the actual values, as shown in Fig. 5. The calculated values are in alignment with the actual values, validating the proposed method for live coupling estimation in CPT systems with multiple receivers.

### B. Experimental validation

A low power experimental setup (up to 10 W) consisting of a single transmitter and one or two receivers, operating at a resonance frequency of 1 MHz, has been realized to validate the proposed method for calculating the mutual capacitance, as shown in Fig. 6.

The circuit is driven by a class-E inverter. The capacitive link is formed using printed circuit boards. The transmitter plate dimensions are set at 300 mm x 300 mm, while the receiver plates measure 145 mm x 300 mm. These plate dimensions were selected based on practical considerations for experimental feasibility and are not the result of an optimization process. The manipulation of the mutual capacitances is achieved by adjusting the distance between the plates and changing their horizontal alignment. These adjustments change the mutual coupling in a manner similar to misalignment in other directions, effectively validating the proposed method under such conditions. Parallel compensation circuits are applied on the primary and secondary sides, using the circuit parameters as listed in Table III.

The mutual capacitances $C_{0n}$ $(n = 1, 2)$ are statically measured according to the theoretical methodology in [21], which will serve as the reference method. This method determines the mutual capacitance by considering the six dominant capacitances in the four-plate capacitive link interface, namely the main coupling capacitances $C_M$, cross-coupling

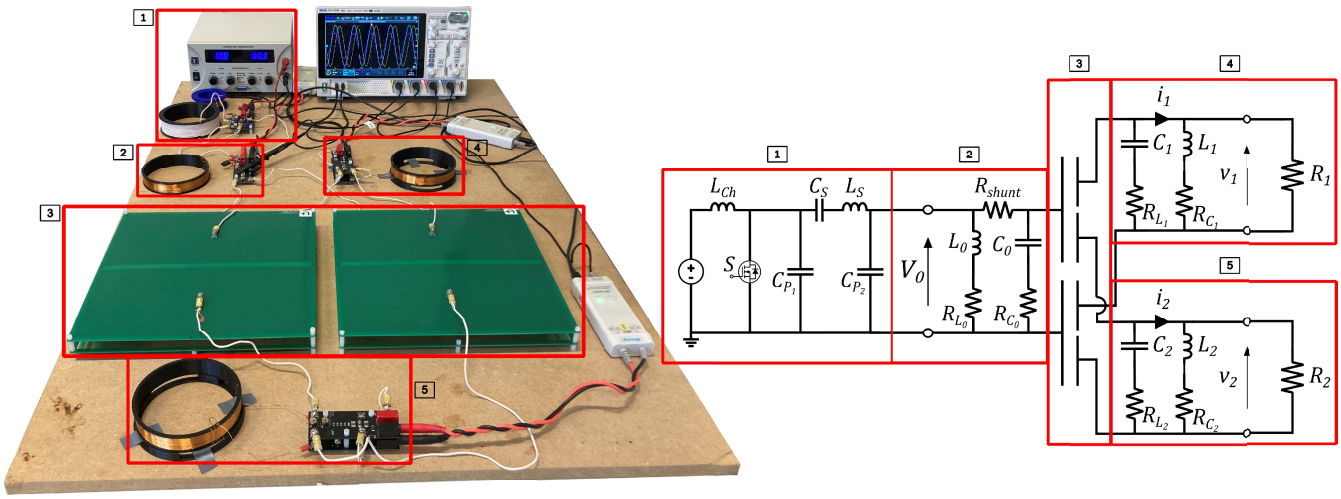


Fig. 6. Measurement setup used for experimental validation and schematic overview of the equivalent circuit with (1) a DC power supply and class-E inverter, (2) the primary parallel compensation circuit, (3) the capacitive link interface, and (4,5) the two secondary compensation circuits with the load resistances $\boldsymbol{R_1}$ and $\boldsymbol{R_2}$. The component values used for the experimental validation are listed in Table III.

TABLE III
VALUES OF EXPERIMENTAL SETUP COMPONENTS FOR THE SISO SYSTEM (SYSTEM 1), THE SIMO SYSTEM WITH EQUAL RECEIVERS (SYSTEM 2) AND THE SIMO SYSTEM WITH UNEQUAL OUTPUT RESISTANCES $R_1$ AND $R_2$ (SYSTEM 3).

| Parameter | System 1 | System 2 | System 3 | Unit |
|---|---|---|---|---|
| $L_0$ | 158.7 | 158.7 | 158.7 | µH |
| $L_1$ | 170.1 | 170.1 | 170.1 | µH |
| $L_2$ | - | 170.5 | 170.5 | µH |
| $R_{L_0}$ | 4.580 | 4.580 | 4.580 | Ω |
| $R_{L_1}$ | 4.920 | 4.920 | 4.920 | Ω |
| $R_{L_2}$ | - | 4.390 | 4.390 | Ω |
| $R_{C_0}$ | 6.120 | 6.120 | 6.120 | Ω |
| $R_{C_1}$ | 6.240 | 6.240 | 6.240 | Ω |
| $R_{C_2}$ | - | 6.844 | 6.844 | Ω |
| $R_1$ | 19.96 | 19.96 | 9.99 | kΩ |
| $R_2$ | - | 19.98 | 19.98 | kΩ |

capacitances $C_C$, and leakage capacitances $C_L$ to construct the resulting $\pi$-equivalent circuit. Since these capacitances cannot be measured individually, the method relies on short-circuiting one of the three capacitances at a time to obtain the sum of the remaining two. By performing three separate measurements, using the IM3536 LCR meter (Hioki, Japan), each capacitance can be determined independently. From these measurements, the mutual capacitances $C_{0n}$ can be calculated using:

$$C_{0n} = \frac{1}{2}\frac{C_M^2 - C_C^2}{C_M + C_C}. \tag{24}$$

The obtained mutual capacitances $C_{0n}$ for each distance between the plates are shown in Table IV.

The controllable compensation capacitances to tune the circuit at a resonant frequency of 1 MHz at different plate distances are realized by incorporating trimmer capacitances in the compensation circuits. For each plate distance, the system is tuned by first adjusting the trimmer capacitors at the secondary sides such that the voltage over each load resistance reach a 90° phase shift with the primary side voltage $v_0$.

TABLE IV
MUTUAL CAPACITANCES $C_{0n}$ AS MEASURED USING THE REFERENCE METHOD FOR THE SISO AND SIMO CONFIGURATIONS AT DIFFERENT VERTICAL PLATE DISTANCES.

| Distance [mm] | Mutual capacitance $C_{0n}$ [pF] | | |
|---|---|---|---|
| | SISO | Receiver 1 | Receiver 2 |
| 5 | 54.195 | 28.653 | 30.853 |
| 6 | 49.313 | 26.090 | 27.958 |
| 7 | 43.203 | 23.455 | 25.468 |
| 8 | 40.780 | 22.215 | 23.910 |
| 9 | 37.090 | 20.483 | 22.445 |
| 10 | 34.198 | 19.005 | 20.278 |
| 11 | 31.605 | 17.628 | 19.370 |
| 12 | 29.613 | 16.348 | 18.430 |
| 13 | 27.705 | 15.718 | 17.243 |
| 14 | 25.983 | 14.660 | 16.480 |
| 15 | 24.503 | 13.800 | 15.558 |
| 16 | 23.568 | 13.333 | 15.095 |
| 17 | 22.503 | 13.213 | 14.258 |
| 18 | 21.623 | 12.438 | 13.893 |
| 19 | 20.383 | 11.780 | 12.710 |
| 20 | 19.553 | 11.238 | 12.390 |

Second, the trimmer capacitor at the primary side is tuned such that the input voltage and current are in phase.

The current at the primary side $i_0$, as indicated in Figs. 2 and 3, is measured using a 100 Ω shunt resistor. The time-domain measurements of $i_0$ and the transmitter and receiver voltages $v_0$, $v_1$ and $v_2$, as shown in Fig. 7, are transformed into their respective phasor representations $\overline{\mathbf{I}}_0$, $\overline{\mathbf{V}}_0$ and $\overline{\mathbf{V}}_n$ by analyzing the amplitude and phase. This transformation uses datasets containing 5000 data points, corresponding to 10 µs of data at a sample frequency of 2 ns. A low-pass filter is used to reduce high-frequency measurement noise.

Instead of directly measuring the currents in the receivers, they are estimated using the phasor representations of the measured receiver voltages $\overline{\mathbf{V}}_n$ and the known electrical parameters of the system:

$$\overline{\mathbf{I}}_n = \overline{\mathbf{V}}_n \left( \frac{1}{j\omega L_n} + \frac{1}{R_n} \right). \tag{25}$$

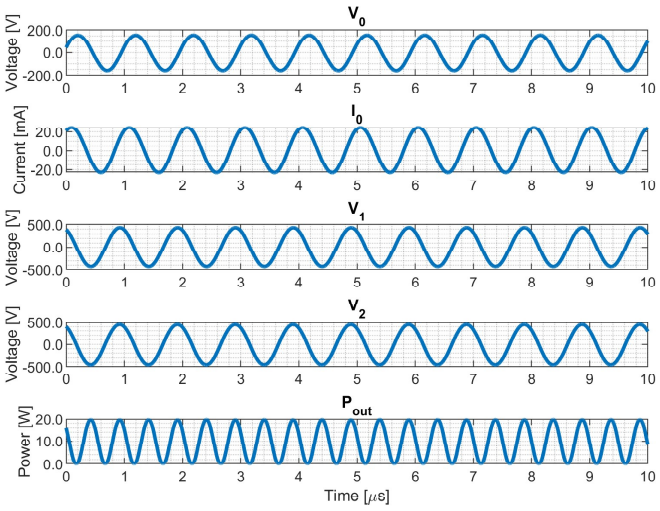


Fig. 7. Time-domain experimental waveforms of the transmitter voltage $v_0$ and current $i_0$, the receiver voltages $v_1$ and $v_2$, and the calculated output power $P_{out}$, captured by the oscilloscope for system 2 at a plate distance of $5\,\mathrm{mm}$.

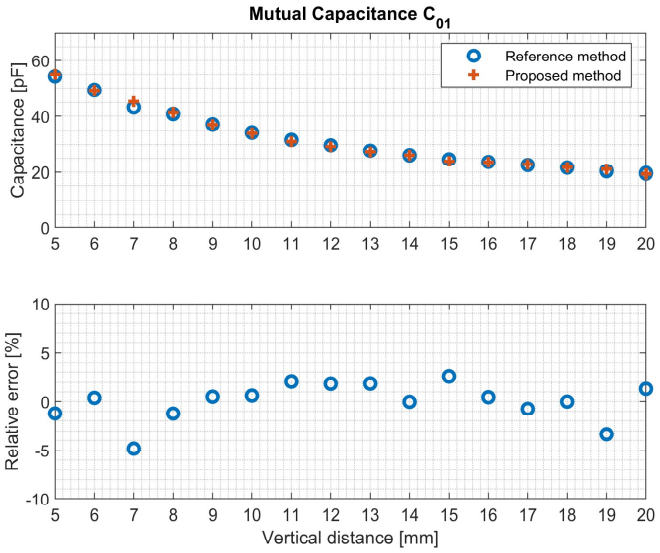


Fig. 8. Measured mutual capacitance $C_{01}$ using the proposed and reference method, and the difference between the two methods as a function of the vertical plate distance for the SISO CPT system (system 1).

In Fig. 8 the measurement results of the proposed method and the reference method [21] are shown for system 1, which is the SISO configuration. It can be seen that the results are similar for the proposed method, validating the correctness of the method. The relative difference between the methods is smaller than $5\,\%$ for all of the data points, which corresponds to an absolute difference smaller than $1\,\mathrm{pF}$ for all of the data points but one. The larger difference at $7\,\mathrm{mm}$ may be caused by imperfections in the manual tuning in the system, or may be due to the measurement uncertainty of both methods.

Fig. 9 presents the measurement results of the proposed method alongside the reference method [21] for system 1 under horizontal misalignment. Similar to the results obtained by varying the vertical distance, the proposed method closely

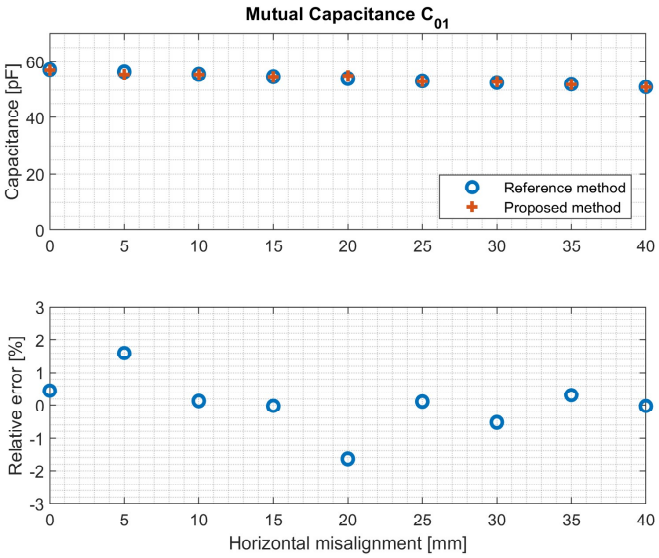


Fig. 9. Measured mutual capacitance $C_{01}$ using the proposed and reference method, and the difference between the two methods as a function of the horizontal plate misalignment for the SISO CPT system (system 1).

matches the reference method, validating its accuracy and demonstrating that the method remains valid for any type of misalignment. The maximum relative error remains below $2\,\%$ for all data points. It should be noted that the change in capacitance due to horizontal misalignment is smaller than that caused by vertical misalignment.

In Fig. 10 the measurement results of the proposed method and the reference method [21] are shown for system 2, which is the SIMO system with equal output resistances $R_1$ and $R_2$. For the first receiver, the relative error between the two methods is less than $5\,\%$ for all of the data points, corresponding to an absolute error of less than $1\,\mathrm{pF}$. For the second receiver, the absolute difference is larger than one pF at 5, 14 and $16\,\mathrm{mm}$. For all of the data points, the proposed method shows a small underestimation compared to the reference method.

In Fig. 11 the measurement results of the proposed method and the reference method [21] are shown for system 3, which is the SIMO system with unequal output resistances $R_1$ and $R_2$. Although still relatively small, the relative difference between the proposed method and the reference method is larger compared to the relative error between the two methods observed for system 1 and 2. This is due to the cross coupling between the receivers, which we have assumed negligible. Because of the larger difference in output voltages $v_1$ and $v_2$, current flows from the second receiver to the first receiver through this cross coupling, resulting in a overestimation of the first receiver's mutual capacitance $C_{01}$, and a underestimation of the second receiver's mutual capacitance $C_{02}$. In future work, this cross coupling between the receivers can be looked into to further improve the results for systems with different receivers.

A significant advantage of the proposed method is its general applicability in CPT systems with various configurations. This robustness stems from the fact that the method relies solely on constant circuit parameters and time-varying voltage and current measurements associated with the ca-

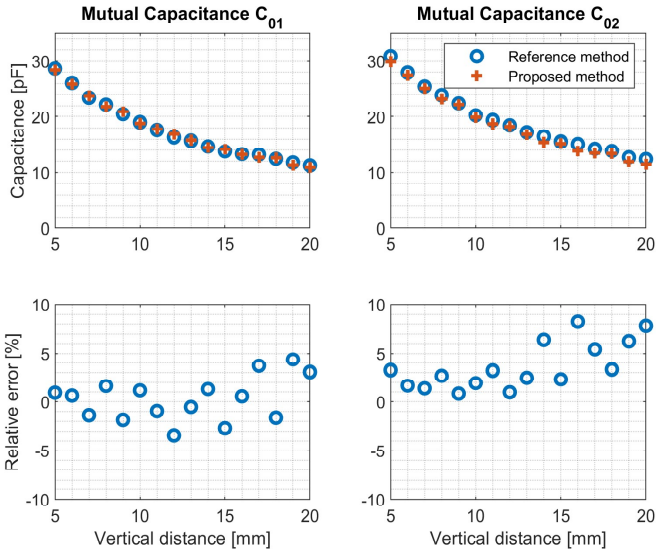


Fig. 10. Measured mutual capacitances $C_{01}$ and $C_{02}$ using the proposed and reference method, and the difference between the two methods as a function of the vertical plate distance for the SIMO CPT system with equal receivers (system 2).

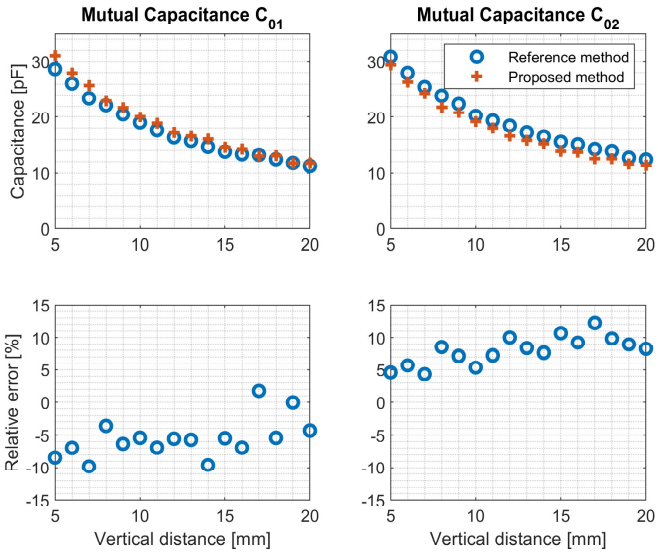


Fig. 11. Measured mutual capacitances $C_{01}$ and $C_{02}$ using the proposed and reference method, and the difference between the two methods as a function of the vertical plate distance for the SIMO CPT system with unequal output resistances $R_1$ and $R_2$ (system 3).

pacitive coupler, without requiring information about specific compensations circuits used. Since the compensation circuit is excluded from the calculations, the method is inherently independent of the type of resonance or impedance-matching network employed. This flexibility makes the approach suitable for a wide range of CPT systems, irrespective of the compensation topology, enabling its use in diverse applications and configurations without significant modifications.

A limitation of the proposed live calculation method is that it requires measuring voltage and current at both the transmitter and receiver, necessitating communication between the two sides. This introduces practical challenges such as phase synchronization, latency, and bandwidth constraints. However, data transmission requirements can be minimized through local phase estimation and onboard processing. Phase synchronization can be achieved by leveraging the resonance condition, where the transmitter and receiver voltages are inherently close to $90°$ apart due to the low series resistance of the capacitive coupler, an essential characteristic for efficient WPT. While communication remains a constraint, these approaches demonstrate that real-time implementation is feasible with appropriate system design. Future work will focus on integrating efficient communication methods to further improve the practicality of the proposed approach.

Another practical consideration is the measurement of the phase angles. A common approach is to use high-speed comparators to generate square-wave signals from the voltage and current waveforms. These signals can then be processed by a phase detector circuit, such as an XOR gate, to determine the phase difference. Alternatively, a high-bandwidth differential op-amp can be used to compare the two signals directly and extract the phase shift. These analog techniques offer a compact and low-latency solution without requiring complex digital processing. While phase measurement was not included in the experimental validation, these methods provide a practical approach for real-world implementations. Future work will explore integrating analog phase detection into a complete CPT system.

Measurement noise can impact both the phase and magnitude of the voltage and current signals, affecting the accuracy of mutual capacitance estimation. One way to reduce the influence of noise is by leveraging the fact that the control loop typically operates at a much lower frequency than the system's operating frequency of $1\,\mathrm{MHz}$. This allows multiple calculations within each control cycle, enabling averaging to minimize random variations. Additionally, circuit design improvements such as low-pass filtering, proper grounding, and shielding can further reduce noise interference, enhancing robustness in practical implementations.

## IV. Conclusion

In this paper, we propose and demonstrate a method for live calculation of the mutual capacitances in SISO CPT systems and SIMO CPT systems with an arbitrary number of receivers. The method derives the mutual capacitances using voltages and currents measurable during normal system operation. Analytical analysis of various system configurations confirms the feasibility of the approach. It is shown that the method is applicable to SISO and SIMO configurations, which is confirmed by simulation and experimental validation.

The results obtained with the proposed method correspond well with those from an established method in the literature [21]. This is particularly true for SISO CPT systems and SIMO CPT systems with identical receivers, where the results are nearly equivalent. However, for SIMO systems with non-identical receivers (e.g. receivers with varying loads), the cross-coupling between receivers can significantly influence the mutual capacitance calculation using the proposed method.

The proposed method can be further improved by taking non-idealities, such as equivalent series resistances into

account. Further research include extending the method for MIMO CPT systems and implementing on board current and voltage measurements along with wireless communication to enable the system to function autonomously.

## ACKNOWLEDGMENTS

This work was supported by a grand from the Research Foundation Flanders (FWO) under Grant Number 1SH1224N.

## DATA SHARING

Data sharing is not applicable to this article as no new data were created or analyzed in this study.

## REFERENCES

[1] X. Mou, D. Gladwin, J. Jiang, K. Li, and Z. Yang, "Near-field wireless power transfer technology for unmanned aerial vehicles: A systematical review," *IEEE Journal of Emerging and Selected Topics in Industrial Electronics*, vol. 4, no. 1, pp. 147–158, 2023.

[2] J. H. Kim, B.-S. Lee, J.-H. Lee, S.-H. Lee, C.-B. Park, S.-M. Jung, S.-G. Lee, K.-P. Yi, and J. Baek, "Development of 1-MW inductive power transfer system for a high-speed train," *IEEE Transactions on Industrial Electronics*, vol. 62, no. 10, pp. 6242–6250, 2015.

[3] S. Li and C. C. Mi, "Wireless power transfer for electric vehicle applications," *IEEE Journal of Emerging and Selected Topics in Power Electronics*, vol. 3, no. 1, pp. 4–17, 2015.

[4] Y. Park, S.-T. Koh, J. Lee, H. Kim, J. Choi, S. Ha, C. Kim, and M. Je, "A wireless power and data transfer IC for neural prostheses using a single inductive link with frequency-splitting characteristic," *IEEE Transactions on Biomedical Circuits and Systems*, vol. 15, no. 6, pp. 1306–1319, 2021.

[5] C. Cai, T. Chen, X. Ren, Y. Jiao, X. Liu, C. Li, J. Yu, and S. Wu, "Modeling and design of a transcutaneous resonant capacitive power transfer link for biomedical implants," *IEEE Transactions on Power Electronics*, vol. 40, no. 2, pp. 3726–3737, 2025.

[6] M. Z. Erel, K. C. Bayindir, M. T. Aydemir, S. K. Chaudhary, and J. M. Guerrero, "A comprehensive review on wireless capacitive power transfer technology: Fundamentals and applications," *IEEE Access*, vol. 10, pp. 3116–3143, 2022.

[7] S. Hong, Y. Kim, S. Lee, S. Jeong, B. Sim, H. Kim, J. Song, S. Ahn, and J. Kim, "A frequency-selective EMI reduction method for tightly coupled wireless power transfer systems using resonant frequency control of a shielding coil in smartphone application," *IEEE Transactions on Electromagnetic Compatibility*, vol. 61, no. 6, pp. 2031–2039, 2019.

[8] H. Wang, U. Pratik, A. Jovicic, N. Hasan, and Z. Pantic, "Dynamic wireless charging of medium power and speed electric vehicles," *IEEE Transactions on Vehicular Technology*, vol. 70, no. 12, pp. 12 552–12 566, 2021.

[9] A. Mahesh, B. Chokkalingam, and L. Mihet-Popa, "Inductive wireless power transfer charging for electric vehicles–a review," *IEEE Access*, vol. 9, pp. 137 667–137 713, 2021.

[10] G. A. Covic and J. T. Boys, "Modern trends in inductive power transfer for transportation applications," *IEEE Journal of Emerging and Selected Topics in Power Electronics*, vol. 1, no. 1, pp. 28–41, 2013.

[11] C. Liu and A. P. Hu, "Steady state analysis of a capacitively coupled contactless power transfer system," in *2009 IEEE Energy Conversion Congress and Exposition*, San Jose, CA, USA, 2009, pp. 3233–3238.

[12] G. G. da Silva and C. A. Petry, "Capacitive wireless power transfer system applied to low-power mobile device charging," *International Journal of Electrical Energy*, vol. 3, 2015.

[13] D. Shmilovitz, S. Ozeri, and M. M. Ehsani, "A resonant LED driver with capacitive power transfer," in *Conference Proceedings - IEEE Applied Power Electronics Conference and Exposition - APEC*. Fort Worth, TX, USA: Institute of Electrical and Electronics Engineers Inc., 2014, pp. 1384–1387.

[14] X. Lv, X. Dai, F. Yu, X. Li, H. Wang, Y. Sun, and J. Hu, "A high misalignment tolerance SCC-WPT system with relay single capacitive coupler for UAV wireless charging applications," *IEEE Transactions on Power Electronics*, pp. 1–6, 2025.

[15] S. Kodeeswaran, M. Nandhini Gayathri, A. Kannabhiran, S. Padmanaban, and P. Carbone, "An electrified tramway wireless charging system for rail transportation using dynamic capacitive power transfer with four vertical plates," *IEEE Transactions on Transportation Electrification*, pp. 1–1, 2025.

[16] J. Dai and D. C. Ludois, "Capacitive power transfer through a conformal bumper for electric vehicle charging," *IEEE Journal of Emerging and Selected Topics in Power Electronics*, vol. 4, pp. 1015–1025, 9 2016.

[17] S. Sinha, A. Kumar, B. Regensburger, and K. K. Afridi, "A new design approach to mitigating the effect of parasitics in capacitive wireless power transfer systems for electric vehicle charging," *IEEE Transactions on Transportation Electrification*, vol. 5, pp. 1040–1059, 12 2019.

[18] S. Bolonne, A. Chanaka, G. Jayawardhana, I. Lionel, and D. Chandima, "Wireless power transmission for multiple devices," in *2016 Moratuwa Engineering Research Conference (MERCon)*, Moratuwa, Sri Lanka, 2016, pp. 242–247.

[19] A. Sokolovs, D. Stepins, and J. Zakis, "Dynamic wireless power transfer system for multiple automated guided vehicles," in *2024 IEEE 11th Workshop on Advances in Information, Electronic and Electrical Engineering (AIEEE)*, Valmiera, Latvia, 2024, pp. 1–4.

[20] W. Zhou, M. Li, Q. Zhang, Z. Li, S. Xie, and Y. Fan, "Potential and challenges of capacitive power transfer systems for wireless EV charging: A review of key technologies," *Green Energy and Intelligent Transportation*, vol. 3, no. 6, p. 100174, 2024.

[21] L. Huang and A. P. Hu, "Defining the mutual coupling of capacitive power transfer for wireless power transfer," *Electronics Letters*, vol. 51, pp. 1806–1807, 10 2015.

[22] W. Zhou, L. Huang, B. Luo, R. Mai, Z. He, and A. P. Hu, "A general mutual coupling model of MIMO capacitive coupling interface with arbitrary number of ports," *IEEE Transactions on Power Electronics*, vol. 36, pp. 6163–6167, 6 2021.

[23] M. Dionigi, M. Mongiardo, G. Monti, and R. Perfetti, "Modelling of wireless power transfer links based on capacitive coupling," *International Journal of Numerical Modelling: Electronic Networks, Devices and Fields*, vol. 30, May 2017.

[24] B. Minnaert, A. Costanzo, G. Monti, and M. Mongiardo, "Capacitive wireless power transfer with multiple transmitters: Efficiency optimization," *Energies*, vol. 13, 7 2020.

[25] S. Sinha, A. Kumar, S. Pervaiz, B. Regensburger, and K. K. Afridi, "Design of efficient matching networks for capacitive wireless power transfer systems," in *2016 IEEE 17th Workshop on Control and Modeling for Power Electronics (COMPEL)*, Trondheim, Norway, 2016, pp. 1–7.

[26] D.-H. Kim and D. Ahn, "Optimization of capacitive wireless power transfer system for maximum efficiency," *Journal of Electrical Engineering & Technology*, vol. 15, no. 1, pp. 343–352, 2019.

[27] K. Doubleday, A. Kumar, B. Regensburger, S. Pervaiz, S. Sinha, Z. Popovic, and K. K. Afridi, "Multi-objective optimization of capacitive wireless power transfer systems for electric vehicle charging," in *2017 IEEE 18th Workshop on Control and Modeling for Power Electronics (COMPEL)*, Stanford, CA, USA, 2017, pp. 1–8.

[28] X. Li, X. Dai, Y. Li, Y. Sun, Z. Ye, and Z. Wang, "Coupling coefficient identification for maximum power transfer in WPT system via impedance matching," in *2016 IEEE PELS Workshop on Emerging Technologies: Wireless Power Transfer (WoW)*, Knoxville, TN, USA, 2016, pp. 27–30.

[29] K. Yue, Y. Liu, P. Zhao, B. Xue, and R. He, "Time domain coupling coefficient estimation using transmitter-side information in wireless power transfer system," in *IECON 2019 - 45th Annual Conference of the IEEE Industrial Electronics Society*, vol. 1, Lisbon, Portugal, 2019, pp. 4189–4194.

[30] K. Yue, Y. Liu, P. Zhao, M. Fu, H. Wang, and J. Liang, "Coupling coefficient and load estimation for wireless power transfer systems with transmitter side input current." Institute of Electrical and Electronics Engineers Inc., 6 2021, pp. 709–713.

[31] X. Dai, X. Li, and Y. Li, "Cross-coupling coefficient estimation between multi-receivers in WPT system," in *2017 IEEE PELS Workshop on Emerging Technologies: Wireless Power Transfer (WoW)*, Chongqing, China, 2017, pp. 1–4.

[32] K. Yue, Y. Liu, X. Zhang, M. Fu, J. Liang, and H. Wang, "Transmitter-side voltage-based mutual inductances and load tracking for two-transmitter LCC-S compensated wireless power transfer systems," *IEEE Journal of Emerging and Selected Topics in Power Electronics*, vol. 12, no. 2, pp. 2317–2332, 2024.

[33] A. van Ieperen, S. Derammelaere, and B. Minnaert, "Live coupling coefficient calculation method for capacitive wireless power transfer with multiple receivers," in *2024 IEEE Wireless Power Technology*

*Conference and Expo (WPTCE)*, San Diego, CA, USA, 2024, pp. 322–325.

[34] L. Murliky, R. W. Porto, V. J. Brusamarello, F. Rangel de Sousa, and A. Triviño-Cabrera, "Active tuning of wireless power transfer system for compensating coil misalignment and variable load conditions," *AEU - International Journal of Electronics and Communications*, vol. 119, p. 153166, 2020.

[35] J. P. Alegre, S. Celma, B. Calvo, and J. M. Garcia del Pozo, "Design of a novel envelope detector for fast-settling circuits," *IEEE Transactions on Instrumentation and Measurement*, vol. 57, no. 1, pp. 4–9, 2008.

[36] Y. Zhou, G. Huang, S. Nam, and B.-S. Kim, "A novel wide-band envelope detector," in *2008 IEEE Radio Frequency Integrated Circuits Symposium*, Atlanta, GA, USA, 2008, pp. 219–222.

[37] X. Zang, J. Zhao, Y. Lu, and Q. He, "Precision measurement system of high-frequency signal based on equivalent-time sampling," *Electronics*, vol. 11, no. 13, 2022.

[38] Z. Liu, F. C. Lee, Q. Li, and Y. Yang, "Design of GaN-based MHz totem-pole PFC rectifier," *IEEE Journal of Emerging and Selected Topics in Power Electronics*, vol. 4, no. 3, pp. 799–807, 2016.

[39] Q. Huang and A. Q. Huang, "Review of GaN totem-pole bridgeless PFC," *CPSS Transactions on Power Electronics and Applications*, vol. 2, no. 3, pp. 187–196, 2017.